Article

Cell Reports

Genetic Dissection of the Type III-A CRISPR-Cas System Csm Complex Reveals Roles of Individual Subunits

Graphical Abstract

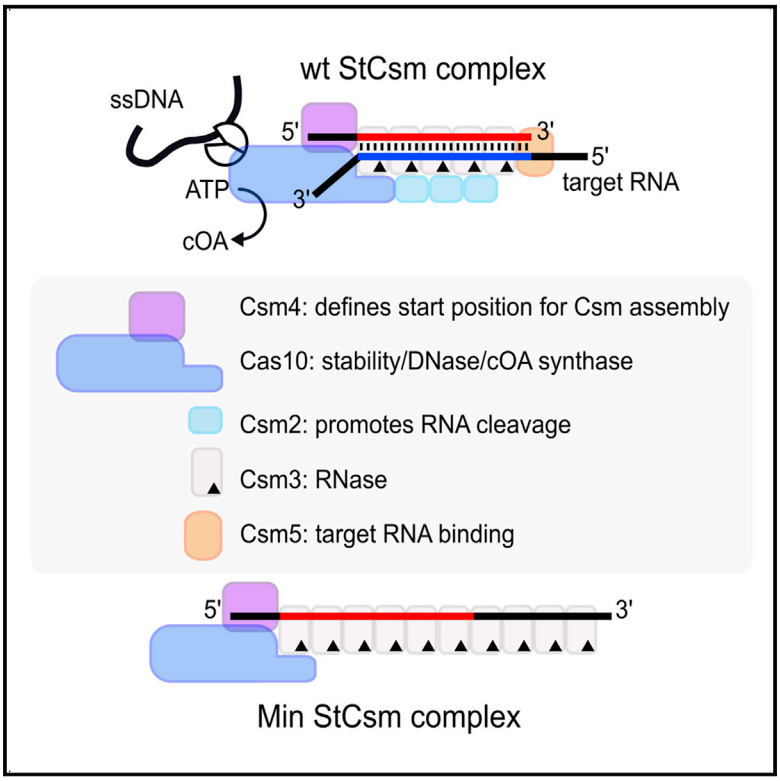

Highlights

- The unmatured Csm complex contains Cas6 at the crRNA 3′-side similarly to type I Cascade
- The Csm4-Cas10 subcomplex binds the crRNA 5′-handle and triggers Csm3 oligomerization
- Csm5, which displaces Cas6 during maturation, is crucial for efficient target RNA binding
- Csm2 promotes target RNA cleavage by Csm3 at multiple sites

Authors

Irmantas Mogila, Migle Kazlauskiene, Skaiste Valinskyte, Giedre Tamulaitiene, Gintautas Tamulaitis, Virginijus Siksnys

Correspondence

tamulaitis@ibt.lt (G.T.), siksnys@ibt.lt (V.S.)

In Brief

Mogila et al. characterized individual subunits of the CRISPR-Cas type III-A Csm effector complex to determine their role in complex assembly and function. A designed minimal Csm complex composed of three subunits (Cas10, Csm3, and Csm4) and a crRNA retains all the functions of the wild-type Csm complex.

Mogila et al., 2019, Cell Reports *26*, 2753–2765
March 5, 2019
https://doi.org/10.1016/j.celrep.2019.02.029

CellPress

Cell Reports
Article

Genetic Dissection of the Type III-A CRISPR-Cas System Csm Complex Reveals Roles of Individual Subunits

Irmantas Mogila,[1] Migle Kazlauskiene,[1] Skaiste Valinskyte,[1,2] Giedre Tamulaitiene,[1] Gintautas Tamulaitis,[1,*] and Virginijus Siksnys[1,3,*]
[1]Institute of Biotechnology, Vilnius University, Saulėtekio av. 7, 10257 Vilnius, Lithuania
[2]Present address: Thermo Fisher Scientific Baltics, Graiciuno 8, 02241 Vilnius, Lithuania
[3]Lead Contact
*Correspondence: tamulaitis@ibt.lt (G.T.), siksnys@ibt.lt (V.S.)
https://doi.org/10.1016/j.celrep.2019.02.029

SUMMARY

The type III-A Csm complex of *Streptococcus thermophilus* (StCsm) provides immunity against invading nucleic acids through the coordinated action of three catalytic domains: RNase (Csm3), ssDNase (Cas10-HD), and cyclic oligoadenylates synthase (Cas10-Palm). The matured StCsm complex is composed of Cas10:Csm2:Csm3:Csm4:Csm5 subunits and 40-nt CRISPR RNA (crRNA). We have carried out gene disruptions for each subunit and isolated deletion complexes to reveal the role of individual subunits in complex assembly and function. We show that the Cas10-Csm4 subcomplex binds the 5′-handle of crRNA and triggers Csm3 oligomerization to form a padlock for crRNA binding. We demonstrate that Csm5 plays a key role in target RNA binding while Csm2 ensures RNA cleavage at multiple sites by Csm3. Finally, guided by deletion analysis, we engineered a minimal Csm complex containing only the Csm3, Csm4, and Cas10 subunits and crRNA and demonstrated that it retains all three catalytic activities, thus paving the way for practical applications.

INTRODUCTION

CRISPR-Cas systems provide prokaryotes with an adaptive immunity against viral and plasmid-derived nucleic acids (NAs) (Koonin et al., 2017). Upon invasion of foreign NAs, short fragments of alien NAs (called protospacers) are acquired by the CRISPR-Cas machinery. These elements are stored as spacers separated by conserved "repeat" sequences in the CRISPR array in the host genome. The CRISPR array serves as a template to generate a pre-CRISPR RNA (pre-crRNA), which is further processed to yield individual crRNA molecules (Charpentier et al., 2015; Hochstrasser and Doudna, 2015). These RNAs form effector complexes with Cas proteins and guide them to specifically destroy invading NAs during subsequent infections. Depending on the composition of the effector complexes, CRISPR-Cas systems are divided into two classes: class 1 systems utilize multisubunit effector complexes, as exemplified by the Cascade complex of type IE system (Sinkunas et al., 2013; Westra et al., 2012), whereas class 2 systems employ single protein effectors, as exemplified by the Cas9 complex (Gasiunas et al., 2012; Jinek et al., 2012). Each class is further subdivided into three types and several subtypes (Koonin et al., 2017).

The immunity of class 1 type III CRISPR-Cas systems is mediated by the multisubunit Csm (type III-A) or Cmr (type III-B) effector complexes that are structurally similar (Benda et al., 2014; Osawa et al., 2015; Rouillon et al., 2013; Spilman et al., 2013; Staals et al., 2013; Taylor et al., 2015) and share a common architecture with the type I-E Cascade complex (Jackson and Wiedenheft, 2015). In type III effector complexes, a large multidomain protein of the Cas10 family (Csm1 in III-A and Cmr2 in III-B) forms the core of the complex, with two intertwined helical protein filaments emerging from it (Osawa et al., 2015; Tamulaitis et al., 2017). The major filament is composed of a single copy of the Csm4 or Cmr3 subunit that anchors the so-called 5′-handle of the crRNA as well as multiple copies of Csm3 or Cmr4 that make a padlock for crRNA binding (Osawa et al., 2015; Tamulaitis et al., 2017). The minor filament is composed of the Csm2 or Cmr5 minor subunits that share a common protein fold with the Cas10 D4 domain (Venclovas, 2016). The structurally similar type I Cascade complex is capped by a Cas6 subunit, which binds to the repeat-derived 3′ end of the crRNA (Hochstrasser and Doudna, 2015; Jackson and Wiedenheft, 2015). Type I and III systems utilize Cas6 for the pre-crRNA cleavage to produce a ~70-nt intermediate (Carte et al., 2008; Hatoum-Aslan et al., 2014); however, the repeat-derived 3′ end of type III crRNA is further processed by non-Cas nucleases to generate matured ~40- to 50-nt crRNAs (Walker et al., 2017). Thus, Cas6 is not present in mature Csm or Cmr complexes. Instead, the 3′ end of crRNA in these complexes is capped by the Csm5 or Cmr1 and Cmr6 subunits, respectively (Tamulaitis et al., 2017).

A transcription-dependent DNA degradation mechanism has been proposed for type III CRISPR-Cas immunity (Samai et al., 2015; Tamulaitis et al., 2017). When phages infect a host cell, transcription of phage DNA is initiated. The Csm or Cmr complex, guided by its crRNA, locates the target sequence in the invasive transcript and binds it, forming a ternary complex. Target RNA binding by Csm or Cmr complex triggers three catalytic activities. First, the Csm3 and Cmr4 subunits, respectively,

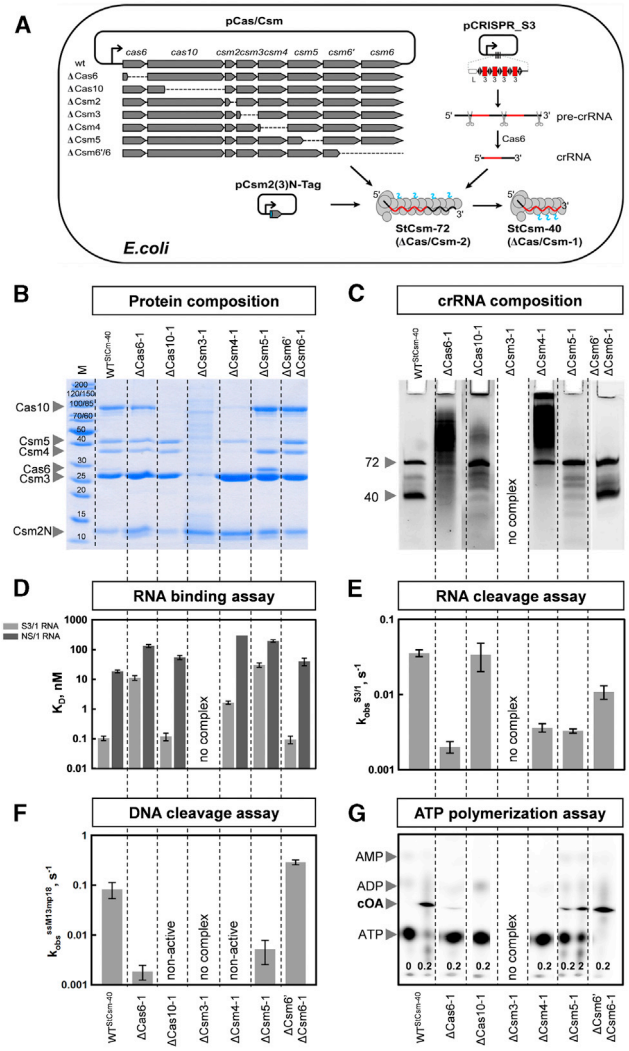

Figure 1. Characterization of ΔCas/Csm-1 StCsm Complexes

(A) Strategy for expression and isolation of WT and deletion mutant variants of the type III-A *S. thermophilus* Csm complex. We isolated two sets of deletion mutant complexes using Csm2-StrepII (ΔCas/Csm-1)- or Csm3-StrepII (ΔCas/Csm-2)-tagged subunits.

(B) Protein composition of the purified StCsm deletion mutant complexes as revealed by SDS-PAGE; M, protein mass marker; Csm2N, N-StrepII-tagged Csm2.

(C) Nucleic acids that co-purified with StCsm deletion mutant complexes.

(D) The dissociation constants (K_D) of specific (S3/1, light bars) and nonspecific (NS/1, dark bars) RNA binding by StCsm deletion mutant complexes.

(E) RNA cleavage rate constant k_{obs} values for StCsm deletion mutant complexes. Reactions contained 4 nM ^{33}P-5′-labeled S3/1 RNA and 160 nM (or 320 nM, in the case of ΔCsm5) StCsm.

(F) DNA degradation rate constant k_{obs} values for deletion mutant complexes. RNA-dependent DNA cleavage reactions contained 2 nM circular ssDNA, 50 nM S3/1 RNA, and 50 nM StCsm.

(G) Synthesis of cOA by deletion mutant complexes. Reactions contained 0 μM or 0.2 μM S3/1 RNA, 0.2 μM StCsm, 50 μM ATP, and 10 nM [α^{32}P]-ATP. For the ΔCsm5-1 mutant, two different concentrations of S3/1 RNA were used (0.2 μM and 2 μM). The concentrations of S3/1 RNA (in μM) used in the reactions are indicated on thin-layer chromatogram.

In (D), (E), and (F), data bars denote mean values from several independent experiments ± SD (standard deviation). See also Figures S1–S3, and S6 and Tables S1–S3.

initiate ribonucleolytic cleavage of the invasive transcript (Tamulaitis et al., 2017); second, the HD domain of Cas10 starts degradation of the single-stranded DNA (ssDNA) in the transcription bubble (Elmore et al., 2016; Estrella et al., 2016; Han et al., 2017; Kazlauskiene et al., 2016; Liu et al., 2017); and third, the Palm domain of Cas10 initiates synthesis of cyclic oligoadenylates (cOAs) (Kazlauskiene et al., 2017; Niewoehner et al., 2017). While the RNase and DNase activities of the Csm or Cmr complex destroy invading NAs, the cOA activates an auxiliary CRISPR-Cas-associated Csm6 or Csx1 ribonucleases, which could destroy an invasive transcriptome at the later stages of phage infection or alternatively might lead to altruistic cell death (Jiang et al., 2016; Kazlauskiene et al., 2017; Koonin and Zhang, 2017; Niewoehner et al., 2017).

The type III-A CRISPR-Cas locus of *Streptococcus thermophilus* DGCC8004 is composed of 13 spacers and 10 *cas/csm* genes (Tamulaitis et al., 2014). Previously, we have expressed the *S. thermophilus* type III-A CRISPR-Cas locus in *Escherichia coli* and isolated two different effector complexes: StCsm-40, which contains a matured 40-nt crRNA, and StCsm-72, which contains an immature 72-nt pre-crRNA resulting from Cas6 cleavage in the repeat sequence (Tamulaitis et al., 2014). These two complexes share a conserved Cas10-Csm4 core but differ in the number of Csm3 and Csm2 subunits. Moreover, the Csm5 subunit is present in StCsm-40 complex containing a matured crRNA but is missing in the StCsm-72 complex (Tamulaitis et al., 2014). While the general function of the catalytic subunits of the Csm complex is already determined, the role of other subunits for the assembly of the complex and its functions remains to be established.

Here, we aimed to determine the role of each StCsm subunit in complex assembly and immunity. We have carried out gene disruptions of each subunit of the Csm and isolated subunit-deletion complexes to reveal the role of individual subunits in the assembly and functions of the complex. To this end, we performed a systematic analysis of *in vitro* activity of different StCsm deletion mutants, including an evaluation of RNA binding, cleavage of target RNA and nonspecific ssDNA, and cOA synthesis.

RESULTS

Complex Composition of StCsm Deletion Variants

StCsm-40 (which contains a 40-nt mature crRNA) and StCsm-72 (which contains a 72-nt immature crRNA) complexes share a conserved set of Cas10, Csm2, Csm3, and Csm4 proteins (Figure 1A) (Tamulaitis et al., 2014). In addition to this core, the mature StCsm-40 complex contains the Csm5 protein. To establish the role of each Csm subunit in the assembly and function of the StCsm complex, we engineered a set of StCsm deletion mutants by disrupting individual *cas/csm* genes in a pCas/Csm plasmid harboring the *cas6-cas10-csm2-csm3-csm4-csm5-csm6′-csm6* gene cassette (Figure 1A; Table S1). The deletion variants were expressed in an heterologous *E. coli* host carrying two additional plasmids: pCRISPR_S3, harboring four (R-S3) repeat-spacer units flanked by the leader sequence and the terminal repeat, and pCsm2N-Tag or pCsm3N-Tag, carrying the StrepII-*csm2* or StrepII-*csm3* genes, respectively (Tamulaitis et al., 2014). To isolate the wild-type (WT) or subunit deletion

Table 1. StCsm Deletion Complexes Used in This Study

Csm Complex	crRNA (nt)	Cas6	Cas10	Csm2	Csm3	Csm4	Csm5
StCsm-40 (WT, "mature")	40	+	+	+	+	+	+
ΔCas6-1	72		+	+	+	+	+
ΔCas10-1	72			+	+	+	+
ΔCsm3-1	–			+			
ΔCsm4-1	72			+	+		+
ΔCsm5-1	72	+	+	+	+	+	
ΔCsm6′6-1	40	+	+	+	+	+	+
StCsm-72 (WT, "immature")	72		+	+	+	+	+
ΔCas6-2	72		+	+	+	+	+
ΔCas10-2	72			+	+	+	+
ΔCsm2-2	72		+		+	+	+
ΔCsm4-2	72			+	+		+
ΔCsm5-2	72		+	+	+	+	
ΔCsm6′6-2	72		+	+	+	+	+

WT StCsm-40 and ΔCsm/Cas-1 StCsm complexes are Csm2 tagged, whereas WT StCsm-72 and ΔCsm/Cas-2 StCsm complexes are Csm3 tagged. A different amount of subunits is present in the complexes. Only the dominant length of crRNA is presented.

complexes, we co-expressed all three plasmids in *E. coli* BL21 (DE3) and pulled down the respective StCsm complexes via StrepII-tags on the Csm2 or Csm3 subunits. Since tagged-Csm2 and tagged-Csm3 pull-downs resulted in two different WT complexes (Csm-40 and StCsm-72, respectively), we characterized the effect of the subunit deletion on the assembly and functional activity of both complexes. We termed the Csm2-tagged StCsm deletion complex variants as ΔCas/Csm-1 complexes and the Csm3-tagged StCsm deletion complex variants as ΔCas/Csm-2 complexes (see Table 1).

First, we examined the protein composition of deletion complexes isolated by Csm2-tagged and Csm3-tagged subunits by SDS-PAGE (Figures 1B and S1B). As expected, the protein corresponding to the disrupted *cas* gene was not present in the pulled-down complexes, and no proteins other than the tagged Csm2 protein were pulled down when the *csm3* gene was deleted (Figure 1B). The yield of all subunit deletion complexes (except for ΔCsm2-2, isolated via the tagged-Csm3 subunit) was lower compared to the WT complexes. The lowest complex yield was observed for ΔCas10 and ΔCsm4 variants (Figure S1A). The deletion analysis suggested that Cas10 is strongly associated with Csm4 in the StCsm complex, since Cas10 was missing in the ΔCsm4 complexes (Figures 1B and S1B). Indeed, using a Cas10-StrepII-tagged variant, we were able to isolate a stable Cas10-Csm4 subcomplex, confirming that Cas10 interacts with the Csm4 subunit (Figures S2A and S2B). Interestingly, the ΔCsm5-1 complex contained the high amount of Cas6 subunit, in contrast to the WT and other complexes (Figure 1B). As expected, the double *csm6′* and *csm6* gene deletion had no impact on StCsm complex composition, since neither of these proteins is present in WT StCsm (Figures 1B and S1B).

We next examined the StCsm complexes for the presence of NAs using phenol-chloroform extraction followed by RNase I or DNase I digestion (Figure S2D). Denaturating PAGE revealed that distinct RNAs co-purified with the different deletion variants of the StCsm complex (Figures 1C and S1C). The ΔCas6 complexes contained long RNAs, consistent with the role of Cas6 in the initial step of pre-crRNA processing (Figures 1C, S1C, and S3). RNA molecules co-purified with the Csm3-tagged ΔCas10-2, ΔCsm2-2, ΔCsm4-2, and ΔCsm5-2 complexes matched the 72-nt immature crRNA that is present in the WT StCsm-72 complex (Figure S1C; Table 1). crRNAs isolated from the Csm2-tagged ΔCas10-1, ΔCsm4-1, and ΔCsm5-1 complexes also matched in length the immature 72-nt species (Figure 1C; Table 1) rather than the 40-nt crRNA present in the WT StCsm-40 complex. The immature 72-nt crRNA and various longer RNAs also purified with both ΔCsm4 complexes (Figures 1C and S1C). Taken together, the data suggest that the Cas10, Csm4, and Csm5 subunits are important for crRNA maturation from 72 nt to 40 nt.

Target RNA Binding by StCsm Deletion Mutants

We next analyzed RNA binding by the StCsm deletion mutants. To monitor binding, we employed an electrophoretic mobility shift assay (EMSA) using two 5′ end radioactively labeled RNAs: target S3/1 RNA, which is complementary to the crRNA in the complex, and a nonspecific NS/1 RNA (Figures 1D and S1D; Table S2). The WT StCsm complex displays a high affinity to the target ssRNA but shows only weak binding to the non-complementary nonspecific RNA (Tamulaitis et al., 2014). EMSA revealed that target RNA binding by the ΔCas10 and ΔCsm2 deletion mutants was as strong as that of the WT complexes. However, the target RNA binding affinity of the ΔCas6 and ΔCsm4 complexes was considerably compromised, presumably due to the low amount of crRNA in the mutant complexes (Figures 1C and S1C; Table S3).

Further analysis revealed that the Csm5 subunit is critical for target RNA binding; the ΔCsm5-1 and ΔCsm5-2 complexes showed, respectively, a ~300-fold and >100-fold decreased binding affinity compared to the WT StCsm complex (Figures 1D and S1D; Table S3). Both ΔCsm5 complexes co-purified with a 72-nt crRNA that is only partially complementary to the S3/1 RNA. To probe whether the compromised binding affinity

of the ΔCsm5 complexes is due to partial complementarity of the RNA target, we next analyzed ΔCsm5 binding to the target RNA fully matching the 72-nt crRNA (S3/6 RNA) (Table S2). While the ΔCsm5-1 complex displayed a moderately increased affinity to the S3/6 RNA, the RNA-binding affinity of both complexes was still significantly lower than that of the WT complexes (Figures 2A and 2B). These results unambiguously show that Csm5 is crucial for target RNA binding by StCsm.

Interestingly, while the binding affinity of the ΔCsm5-2 complex to the 72-nt S3/6 RNA was ~1,000-fold weaker that of the WT StCsm-72 complex, ΔCsm5-1 exhibited only a ~10-fold decreased binding affinity (Figures 2A and 2B). The only difference between ΔCsm5-2 and ΔCsm5-1 complexes is the presence of a significant amount of Cas6 protein in the latter complex (Figures 1B and S1B). This suggests that Cas6 could contribute to RNA binding in the absence of Csm5. ΔCsm5-1 formed a stable complex with nonspecific RNA; however, its mobility differed from the target RNA complex (Figure 2B) and corresponded to a mobility of NS/1 RNA bound to the individual Cas6 protein. Mass spectrometry (MS) of the nonspecific complex confirmed that it contained mostly Cas6 (see text below; Table S4). This finding suggests that Cas6 dissociates from the ΔCsm5-1 complex upon non-target RNA binding but promotes target RNA binding by the ΔCsm5-1 complex. Notably, the target RNA binding affinity of the ΔCsm5 complexes was fully recovered by adding the individual Csm5 protein, which replaced Cas6 in the complex (Figure 2C). Complementation of the ΔCsm5-1 complex with Csm5 resulted in a ~100-fold increase in the binding affinity to the nonspecific NS/1 RNA (bands 1 and 2) and *en masse* release of Cas6 from the complex. The identity of the Cas6 released from the complex in bands 1 and 2 was confirmed by MS analysis (Table S4). Cas6 binding to the 3′ end of immature crRNA in the ΔCsm5-1 complex presumably also compromised target RNA cleavage at 5′ end proximal sites (Figures S4B and S4C). Indeed, ΔCsm5-1 complementation with Csm5 protein restored cleavage at 5′ end proximal sites and produced a cleavage pattern identical to that of WT StCsm (Figure S4D).

Target RNA Cross-Linking to StCsm Deletion Mutants

To determine which StCsm subunits are in direct contact with the heterocyclic bases of the target RNA bound in the complex, we performed UV cross-linking experiments of the WT and ΔCsm5 complexes. We used radiolabeled target (S3/1 and S3/6) and nonspecific (NS/1 and NS/2) RNAs containing photoreactive 4-thiouridine residues (Table S2). The 4-thiouridine and ^{32}P-adenosine were incorporated throughout the entire RNAs substituting U and A, respectively. The StCsm complex bound to the 4-thiouridine-containing RNA target was subjected to UV irradiation followed by RNase treatment and SDS-PAGE analysis. The Csm protein subunits were visualized by Coomassie staining while covalently associated radiolabeled regions of the RNA were identified using autoradiography (Figure S5). In the WT StCsm-40 complex, Cas10, Csm5, and Cas6 were found to be covalently cross-linked to the target (S3/1 and S3/6) RNA. Interestingly, only Csm5 and Cas6, but not Cas10, cross-linked to the nonspecific NS/1 and NS/2 RNAs. The protein cross-linking pattern observed for the ΔCsm5-1 complex was identical to that of the WT complex except for the missing Csm5. The Cas6 cross-links were more pronounced in ΔCsm5-1 compared to WT StCsm-40. In case of the WT StCsm-72 complex, Cas10 and a small fraction of Csm5 and Cas6 (only to S3/1 RNA) cross-linked to the target RNA. A very small amount of Csm5 (but not Cas10) cross-linked to both nonspecific RNAs. Similarly, in the ΔCsm5-2 complex, only Cas10 and, to a lesser extent, Cas6 cross-linked to the target RNA.

RNA Cleavage by StCsm Deletion Mutants

The StCsm complex cleaves complementary target RNA bound in the ternary complex, thus generating a characteristic 6-nt interspaced cleavage pattern (Tamulaitis et al., 2014). To analyze target RNA cleavage by the StCsm deletion complexes, we monitored the cleavage of S3/1 target RNA, which was radioactively labeled at its 5′ end. We then determined the cleavage rate by fitting the measured substrate degradation to an exponential decay model (Figures 1E and S1E; Table S3). Surprisingly, most of the StCsm deletion mutants retained specific RNA cleavage activity and did not hydrolyze nonspecific RNA (Figure S6). The ΔCas10 mutants showed a RNA cleavage activity similar to that of the WT complex. The ΔCas6, ΔCsm4, and ΔCsm5 complexes cleaved RNA inefficiently in agreement with their decreased target RNA binding affinity. While the ΔCas6, ΔCas10, and ΔCsm5 complexes produced a periodic pattern characteristic of WT StCsm cleavage, distinct cleavage patterns were observed for the ΔCsm2 and ΔCsm4 mutants (Figure S6).

The WT StCsm-72 complex cut a fully complementary S3/6 RNA substrate at 10 sites that were regularly spaced by 6-nt intervals (Figure 3A) (Tamulaitis et al., 2014). Although the ΔCsm2-2 complex cut target RNA at all the possible sites, cleavage at the 5′-proximal sites was significantly impaired (Figures S1E and 3A). The ΔCsm2-2 mutant produced one dominant RNA cleavage product resulting from cleavage at the site closest to the 3′ end of the target S3/6 RNA. Furthermore, a couple of minor products resulting from cleavage at 3′-proximal sites were detected. Addition of the individual Csm2 protein to the ΔCsm2-2 complex fully restored the cleavage pattern observed for WT StCsm (Figure 3B).

In contrast, ΔCsm4 complexes produced a multitude of products that each differed by 1 nt (Figure 4A). To confirm the cleavage pattern of ΔCsm4, we constructed a set of RNA substrates that were only partially complementary to the S3 crRNA (substrates S3/20, S3/21, S3/22, and S3/23 in Figure 4). The WT StCsm-72 complex cleaved the mismatched substrates in the spacer region complementary to the crRNA in regular 6-nt intervals (Figures 4B). The ΔCsm4-2 mutant complex cleaved the RNA substrates only in the complementary regions of mismatched RNA substrates but produced a 1-nt ladder of cleavage products in these regions (Figures 4B).

Cas10-Catalyzed Activities of Deletion Mutants

The large subunit Cas10 of the Csm complex (also termed Csm1 in type III-A) is a signature protein of the type III systems (Tamulaitis et al., 2017). Cas10 is a multidomain protein containing an HD nuclease domain that degrades foreign DNA (Kazlauskiene et al., 2016) and two Palm (polymerase/nucleotide cyclase-like) domains that are responsible for synthesizing cOAs (Kazlauskiene et al., 2017). Both activities are triggered in response to the target RNA binding. Since RNA binding is compromised in some of the

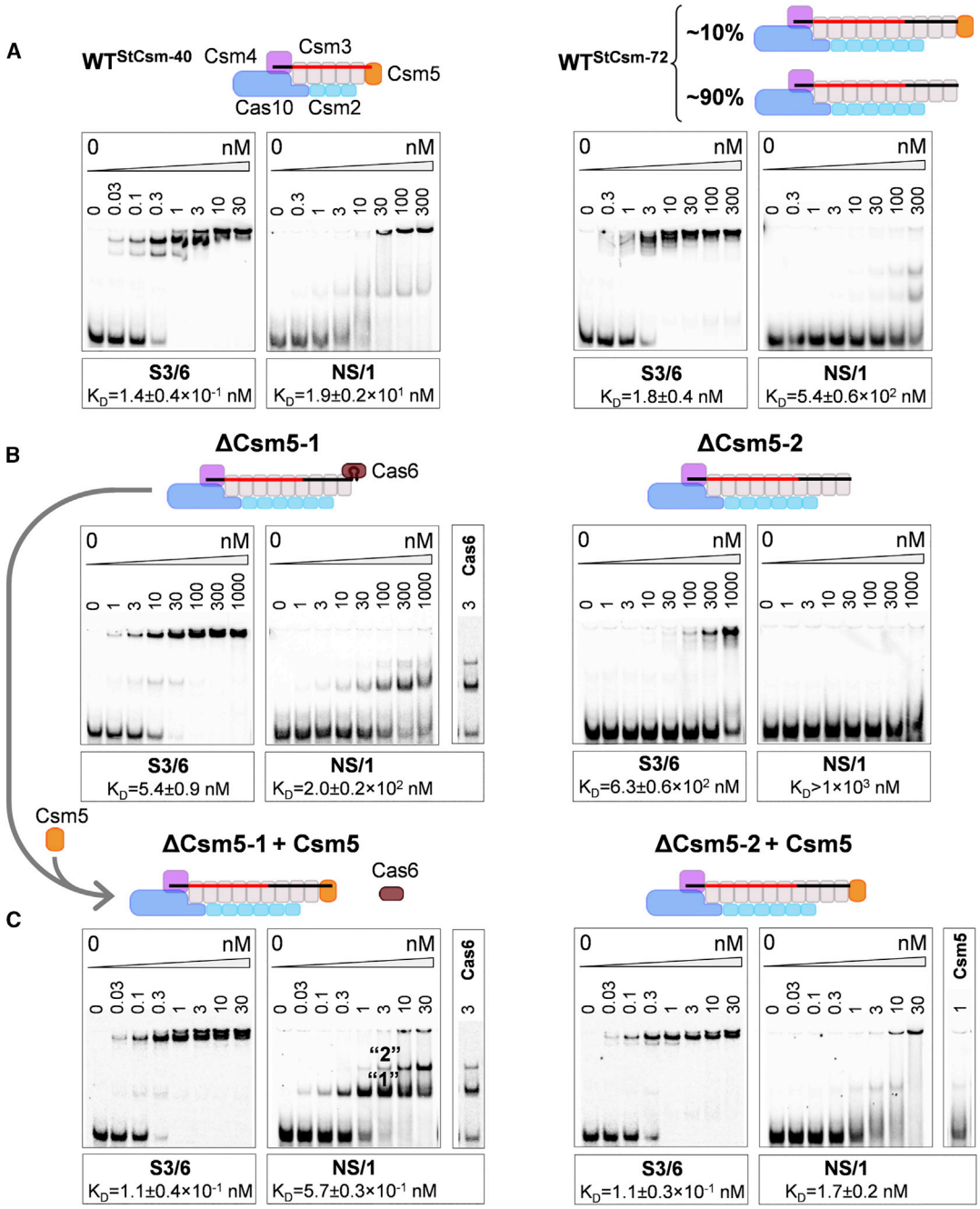

Figure 2. RNA Binding by the ΔCsm5 Deletion Mutant Complex

(A) EMSA analysis of WT StCsm-40 and StCsm-72 complexes.

(B) EMSA analysis of ΔCsm5-1 and ΔCsm5-2 mutant complexes.

(C) EMSA analysis of ΔCsm5 mutant complexes premixed 1:1 with Csm5 protein. "1" and "2" indicate bands that were analyzed by MS.

In (A)–(C), the binding reactions contained ^{33}P-labeled specific S3/6 or nonspecific NS/1 RNA (0.5 nM) and the StCsm at concentrations indicated in each lane. The calculated dissociation constant (K_D; presented as mean ± SD) is indicated below each gel. Control lanes in (B) and (C) contained 3 nM purified Cas6 or Csm5 and 0.5 nM NS/1 RNA. See also Figures S3–S5 and Tables S1 and S4.

StCsm deletion variants, we analyzed the ssDNase and cOA-synthase activity of the deletion variants.

First, we examined whether the binding of the deletion mutants to target RNA can trigger nonspecific M13mp18 ssDNA degradation. The ΔCsm2-2 complex degraded ssDNA at a rate comparable to the respective WT complex. Both ΔCsm5 complexes degraded ssDNA at a significantly slower rate than the WT StCsm-40 complexes, while the ΔCas6 complexes retained

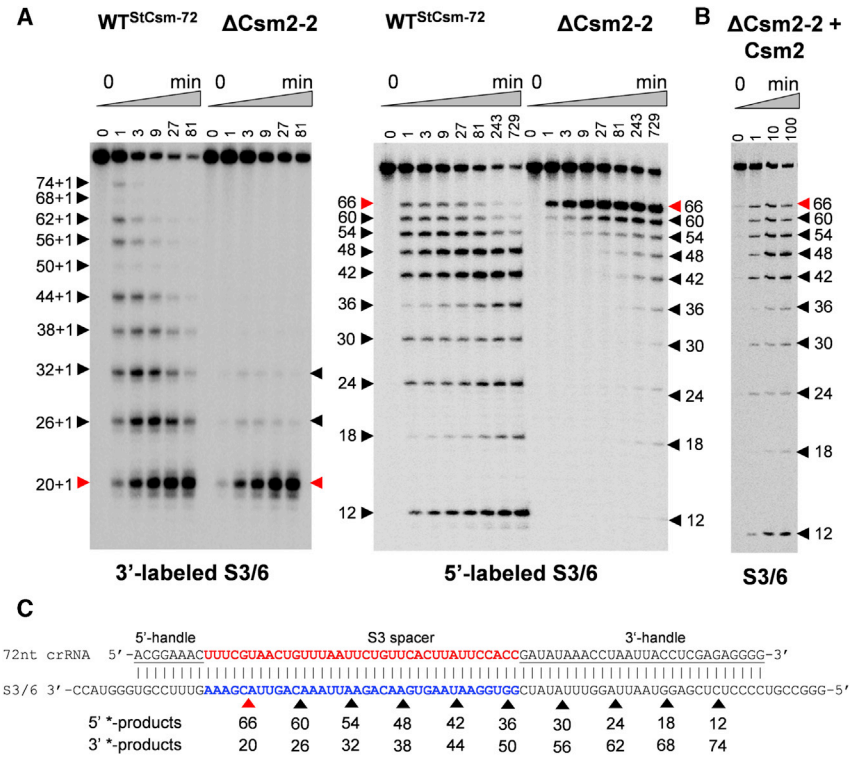

Figure 3. RNA Cleavage by the ΔCsm2 Mutant Complex

(A) S3/6 RNA cleavage assay of WT StCsm-72 and ΔCsm2-2. RNA was 5′ or 3′ end labeled with ^{33}P or ^{32}P and gel purified. Red triangles denote the product originating from cleavage site nearest to 3′ end of target RNA, while black triangles mark remaining products.

(B) ΔCsm2-2 complementation with Csm2 protein. Black triangles indicate cleavage products originating from restored active sites.

(C) Map of S3/6 RNA substrate cleavage positions by the WT StCsm-72 complex.

only weak residual ssDNase activity. These results correlated with impaired binding of the target RNA by the ΔCas6 and ΔCsm5 complexes. The ΔCas10 and ΔCsm4 complexes were unable to degrade DNA (Figures 1F and S1F; Table S3), since Cas10, which is responsible for ssDNA cleavage, was absent in both complexes.

Next, we examined whether binding of the deletion mutants to target RNA could trigger synthesis of cOA signaling molecules from ATP. Reaction products of [α-^{32}P]-labeled ATP were analyzed by thin-layer chromatography (Figures 1G and S1G). As expected, the cOA-synthase activity of the StCsm deletion variants correlated with their DNA degradation activity. The low cOA yield observed for the ΔCsm5-1 mutant was presumably due to impaired target RNA binding. An increase in the S3/1 target RNA concentration in the reaction mix from 0.2 μM to 2 μM increased the cOA yield 3-fold (Figure 1G).

Assembly of a Minimal StCsm Complex

Deletion analysis data revealed that the Csm3 RNase subunit is critical for the StCsm complex assembly (Figure 1B), while Csm4 ensures crRNA binding and positioning in the complex (Figure 4). Taken together, these data show that crRNA, Csm3, and Csm4 are essential components of the complex. Next, we explored the possibility to assemble a minimal StCsm complex composed of only three components. Such an engineered minimal variant of StCsm would be a convenient tool for specific RNA targeting both *in vitro* and *in vivo*.

To obtain a minimal StCsm variant, we constructed a plasmid (pCsm3N-Tag_Csm4) carrying the genes for StrepII-tagged *csm3* and *csm4* and a second plasmid (pCas6) carrying the *cas6* gene. The expression of the Cas6 protein in the context of the pCRISPR_S3 plasmid encoding the CRISPR array would produce a 72-nt crRNA. We then co-expressed pCsm3N-Tag_Csm4, pCas6 and pCRISPR_S3 plasmids in *E. coli* BL21(DE3) and purified the minimal complex. The yield of the obtained complexes was very poor being characteristic for ΔCas10 complexes. Therefore, we included an additional expression plasmid carrying the *cas10* gene (pCas10). The isolated minimal StCsm complex contained Cas10, Csm3, Csm4, and Cas6 and a 72-nt crRNA (Figure S7). To eliminate the Cas6 subunit from the complex, we used a His-tagged Cas6 (pCas6-Tag) and an additional His-chelating chromatography step. This allowed us to isolate the minimal StCsm variant (Min-StCsm) without Cas6. SDS-PAGE of Min-StCsm revealed three bands that matched the individual Cas10, Csm3, and Csm4 proteins (Figure 5A). Denaturing PAGE analysis revealed that an ~70-nt crRNA predominantly co-purified with Min-StCsm (Figure 5B) similarly to the deletion mutant variants that lack the Csm2 and Csm5 subunits. EMSA revealed that the minimal complex bound S3/6 RNA with low affinity, similar to the ΔCsm5-2 mutant (Figure 5C; Table S3). Min-StCsm exhibited a bi-exponential RNA cleavage kinetics indicating the presence of two different complex populations: a fast-cleaving population that cuts close to the 3′ end of the RNA target and a slow-cleaving population that cuts the substrate at the remaining sites (Figure 5D). Overall, the Min-StCsm complex exhibited a ~20-fold decreased RNA cleavage rate at the first cleavage site and a ~1,500-fold decreased rate at the other sites (Table S3). Min-StCsm that contained the Cas10 subunit was still able to cleave ssDNA, albeit at decreased rate (Table S3), and produce cOAs (Figures 5E and 5F).

DISCUSSION

The Architecture of the StCsm Complex Affects crRNA Maturation

By varying the tagged StCsm subunit in the *E. coli* expression system, we have previously isolated two types of StCsm complexes termed StCsm-72 and StCsm-40 (Tamulaitis et al., 2014). Both complexes shared a conserved set of Cas10,

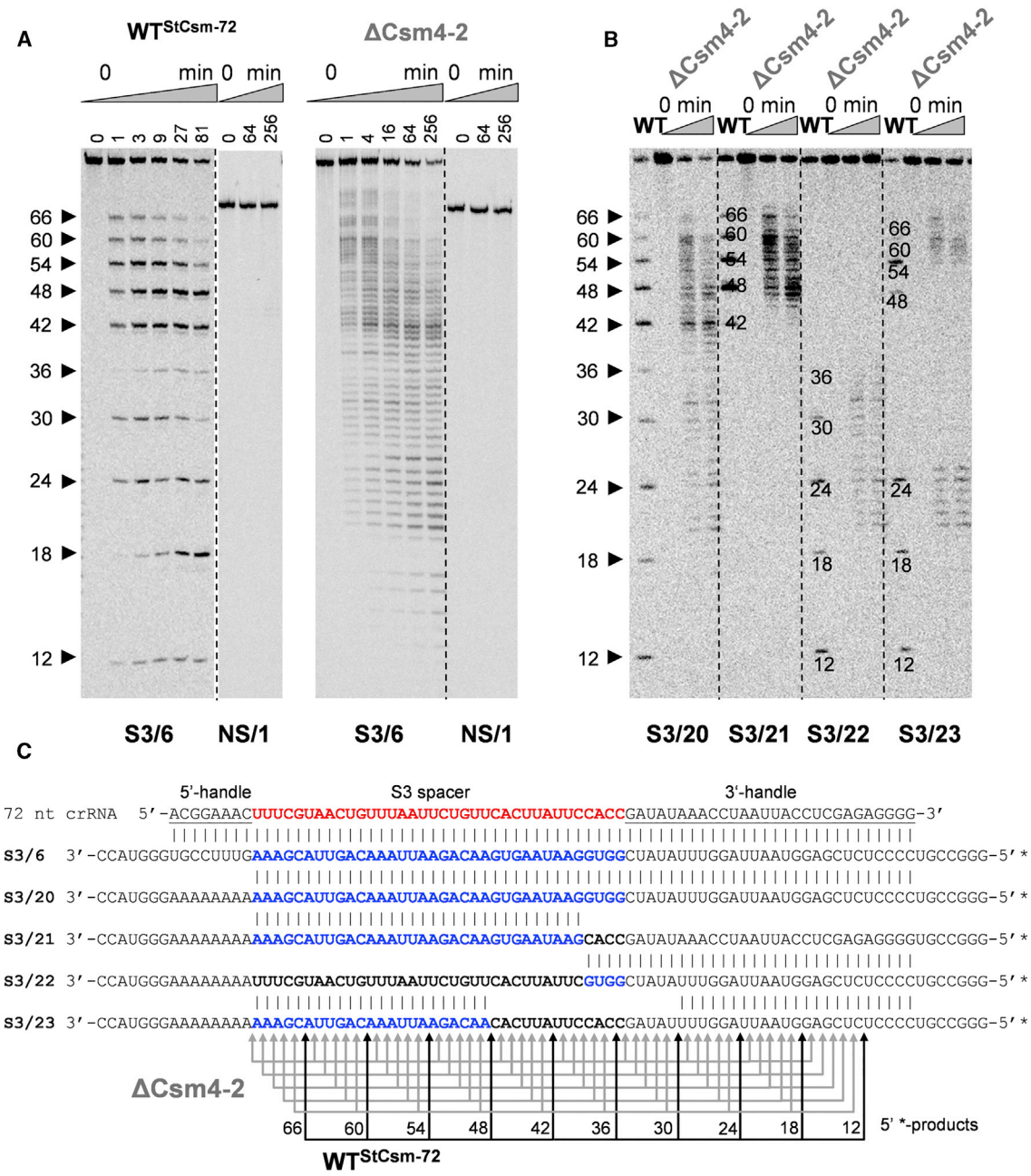

Figure 4. RNA Cleavage by the ΔCsm4 Mutant Complex

(A) RNA cleavage assay of target S3/6 RNA by WT StCsm-72 and ΔCsm4-2.

(B) RNA cleavage assay of target RNA containing different mismatches by WT StCsm-72 and ΔCsm4-2 mutant.

(C) Scheme explaining the RNA cleavage by the WT complex and ΔCsm4 variants. Black connected arrows mark cleavage sites of the WT complex, and gray connected arrows indicate cleavage patterns of different ΔCsm4 mutant complex variants bound to the target RNA. RNA was 5′ end labeled with ^{33}P and gel purified.

Csm2, Csm3, and Csm4 proteins. StCsm-40, but not StCsm-72, also contained the Csm5 subunit. Two distinct crRNAs of 72 nt and 40 nt co-purified with StCsm-72 and StCsm-40, respectively. The 72-nt crRNA, composed of an 8-nt 5′-handle, a 36-nt spacer, and a 28-nt 3′-handle, resulted from the primary CRISPR transcript cleavage within the conserved repeat region by the Cas6 nuclease. The 40-nt crRNA contained the conserved 8-nt 5′-handle and a 32-nt spacer. This indicates that the 72-nt crRNA intermediate undergoes further 3′ end processing to produce a matured 40-nt crRNA that lacks the 3′-handle and a few nucleotides within the spacer region (Tamulaitis et al., 2014). A similar crRNA maturation pattern was found for the

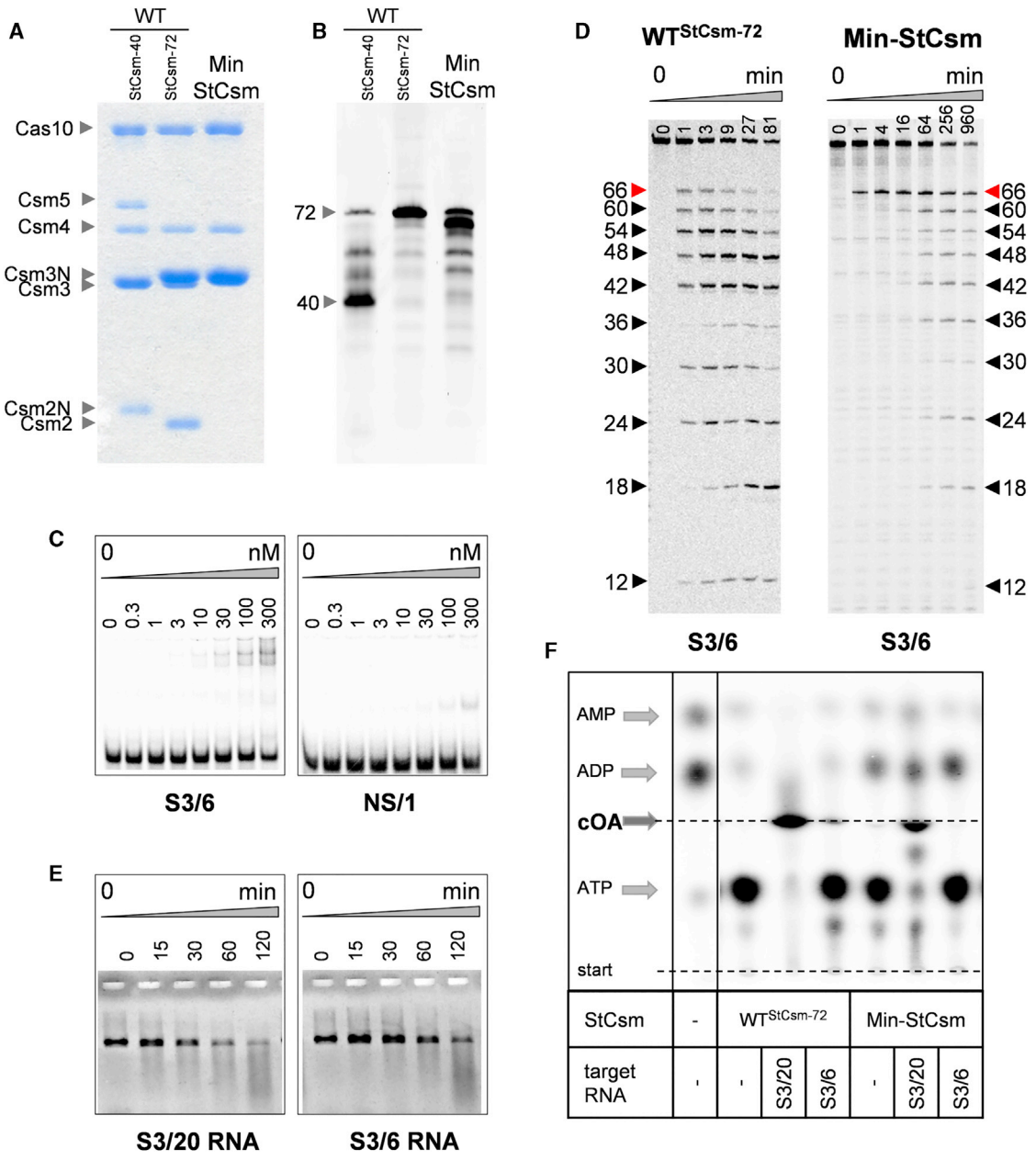

Figure 5. Characterization of the Minimal StCsm Complex

(A) Protein subunits of the Min-StCsm complex as revealed by SDS-PAGE. Csm2N and Csm3N indicate N-StrepII-tagged Csm2 and Csm3, respectively.

(B) crRNA composition of Min-StCsm analyzed by denaturing PAGE.

(C) Min-StCsm complex binding affinity to S3/6 or NS/1 RNA substrates.

(D) ^{33}P-5′-labeled S3/6 RNA substrate cleavage by Min-StCsm.

(E) ssDNA cleavage by Min-StCsm complex.

(F) Synthesis of cOA by Min-StCsm.

StCsm DNase- and cOA-synthase-activating S3/20 RNA and non-activating S3/6 RNA were used in the reactions shown in (E) and (F). See also Tables S1 and S2.

Staphylococcus epidermidis SeCsm complex (Hatoum-Aslan et al., 2011, 2013). While in the *S. epidermidis* type III-A CRISPR-Cas system *cas6*, *cas10*, and *csm4* genes were necessary for the formation of crRNAs (Hatoum-Aslan et al., 2011), we showed here that in the *S. thermophilus* system, Cas10 and Csm4 are important for the crRNA maturation, as the ΔCas10 and ΔCsm4 deletion complexes contained a 72-nt pre-crRNA (Figure 1C). Since deletion of any StCsm subunit impaired the crRNA maturation from 72 nt to 40 nt (Figures 1C and S1C; Table 1), we conclude that Csm complex assembly is obligatory

for crRNA maturation to the 40-nt species. Notably, the yield of the *S. thermophilus* ΔCas10 and ΔCsm4 complexes was extremely low, presumably due to the absence of Cas10 in these variants (Figures 1B, S1A, and S1B). The absence of any crRNA in *S. epidermidis* cells containing Δ*cas10* and Δ*csm4* (Hatoum-Aslan et al., 2011) could also be explained by the low overall yields of the respective complexes. We speculate that for this reason, Hatoum-Aslan et al. (2014) were unable to isolate ΔCas10-SeCsm and ΔCsm4-SeCsm complexes.

Cas6 Is Associated with StCsm during Maturation

In type I and III CRISPR-Cas systems, crRNA is produced by Cas6 cleavage of the pre-crRNA transcript (Charpentier et al., 2015; Hochstrasser and Doudna, 2015). In the I-B, I-E, and I-F Cascade complexes, Cas6 remained bound to the repeat-derived 3′ end of the ~70-nt crRNA (Hochstrasser and Doudna, 2015). In type III CRISPR-Cas systems, pre-crRNA was further processed and Cas6 was absent in the mature complex (Hochstrasser and Doudna, 2015).

We showed here that StCas6 *in vitro* bound the repeat R/1 RNA with high affinity and cleaved it at the base of the predicted stem-loop (Figure S3) similarly to SeCas6 of *S. epidermidis* (Hatoum-Aslan et al., 2014). We found that consistent with previous studies, in the absence of StCas6, the 72-nt crRNA intermediate was not produced, yielding instead StCsm complexes that contained RNAs of various length (Figures 1C and S1C) (Charpentier et al., 2015; Hatoum-Aslan et al., 2011). It is likely that some of these complexes contained the CRISPR-array transcript or its degradation products, since ΔCas6 complexes still showed a weak specific RNase activity and the characteristic 6-nt cleavage pattern of S3/1 RNA (Figures 1E, S1E, and S6B).

We further found that Cas6 exhibited high affinity to the repeat cleavage product R/2 RNA (Figure S3A), similarly to PfCas6 from *Pyrococcus furiosus* type III-B system (Carte et al., 2008). Therefore we hypothesize that the type III effector complexes undergo a Cascade-like maturation stage during which Cas6-bound ~70-nt crRNA is incorporated into the immature Csm or Cmr complexes, as exemplified by the ΔCsm5-1 complex containing bound Cas6 (Figure 1B; Table 1). A different crRNA maturation pathway that does not involve crRNA 3′ end processing after Cas6 cleavage has been reported recently for the type III-A CRISPR-Cas system from *Mycobacterium tuberculosis* (Wei et al., 2019).

Our previous data showed that the Csm3 expression level in cells influences the maturation of crRNA in the StCsm complex similarly to the *S. epidermidis* type III-A CRISPR-Cas system (Hatoum-Aslan et al., 2013; Tamulaitis et al., 2014). The overexpression of StCsm3 yielded 72-nt crRNAs in StCsm-72, while overexpression of SeCsm3 resulted in a shift in the crRNA size toward larger species in SeCsm. According to MS analysis, both StCsm-40 and StCsm-72 complexes contained a Cas6 subunit (Tamulaitis et al., 2014), but the amount of Cas6 differed between the complexes. In StCsm-40 samples, ~10% of the complexes contained Cas6 and a 72-nt crRNA, indicating that ~10% of immature complexes co-purified with StCsm-40 (Tamulaitis et al., 2014). In the StCsm-72 complex, only traces of Cas6 undetectable in SDS-PAGE were present according to MS analysis, since overexpression of Csm3 resulted in the displacement of Cas6. The use of a low-copy-number plasmid for Csm3 expression in preparation of the minimal StCsm complex produced complexes that still contained Cas6 bound to the immature 72-nt crRNA in the complex (Figure S7).

Random RNA Target Cleavage Pattern by ΔCsm4 Complexes

Interestingly, all of the Csm3-containing deletion mutants retained a characteristic RNA cleavage pattern, except for ΔCsm4 (Figure S6B). Unlike WT StCsm, which cleaves target RNA with regular 6-nt periodicity, the ΔCsm4 mutant reaction products are interspaced by 1 nt (Figure 4). Cmr3, the ortholog of Csm4, was shown to specifically recognize and bind the 5′-handle of crRNA (Osawa et al., 2015) presumably defining the start of the complex assembly. We assume that in the absence of Csm4, the position of the 5′-handle of crRNA is not defined, resulting in a mixed complex population containing randomly bound crRNAs that differ in the register of Csm3 ribonucleases with respect to crRNA (Figure 4C). Csm3 oligomers in these random complexes each cleave the target RNA in regular 6-nt patterns, producing a resultant 1-nt cleavage pattern. When expressed alone, Csm3 still purifies with various RNAs (Figure S2C), emphasizing its high affinity toward RNA. Similarly, recombinant SeCsm3 binds nonspecific RNA molecules at multiple sites, with each SeCsm3 protein interacting with 6 nt of the RNA (Hatoum-Aslan et al., 2013). Since overproduced 72-nt pre-crRNA is one of the most abundant short RNA species in the cell, Csm3 binds it during ΔCsm4 complex assembly.

Csm2 Promotes RNA Cleavage by Csm3 Subunits

The small subunit Csm2 forms the minor filament that intertwines with the larger Csm3 filament in the Csm complex, bit the functional role of Csm2 remained obscure (Tamulaitis et al., 2017). In the Cmr complex, Cmr5 (a Csm2 equivalent) is positioned near the scissile phosphodiester bond and could contribute to the correct orientation of the target RNA in the RNase active site of the Cmr4 (Csm3) subunit (Osawa et al., 2015). Biochemical analysis of the ΔCsm2 mutants of the StCsm complex provided experimental support for this hypothesis. EMSA and cleavage experiments revealed that Csm2 has no impact on target RNA binding (Figure S1D) but is required for efficient RNA cleavage at multiple sites. In contrast to the WT StCsm-72 that cut target RNA at 10 sites, the ΔCsm2-2 mutant cut efficiently only at the first 3′-proximal site and showed much reduced cleavage at the second and the third sites, respectively (Figures 3 and S6B). Since the 3′-proximal site RNA cleavage site is adjacent to the Cas10 D4 domain, which is structurally similar to Csm2 and Cmr5 subunits (Osawa et al., 2015; Venclovas, 2016), it is likely that the D4 domain of Cas10 ensures the correct RNA positioning in the active site of the Csm3 subunit closest to the 5′-handle of crRNA. Importantly, ΔCsm2 complex complementation by addition of the individual Csm2 subunit restored cleavage at all 10 possible sites (Figure 3B). Interestingly, despite a lack of the D4 domain, the ΔCas10 mutant showed a WT cleavage pattern (Figure S6B), suggesting that an extra Csm2 subunit presumably replaced the Cas10 D4 domain and ensured target RNA orientation and interaction with the first Csm3 subunit.

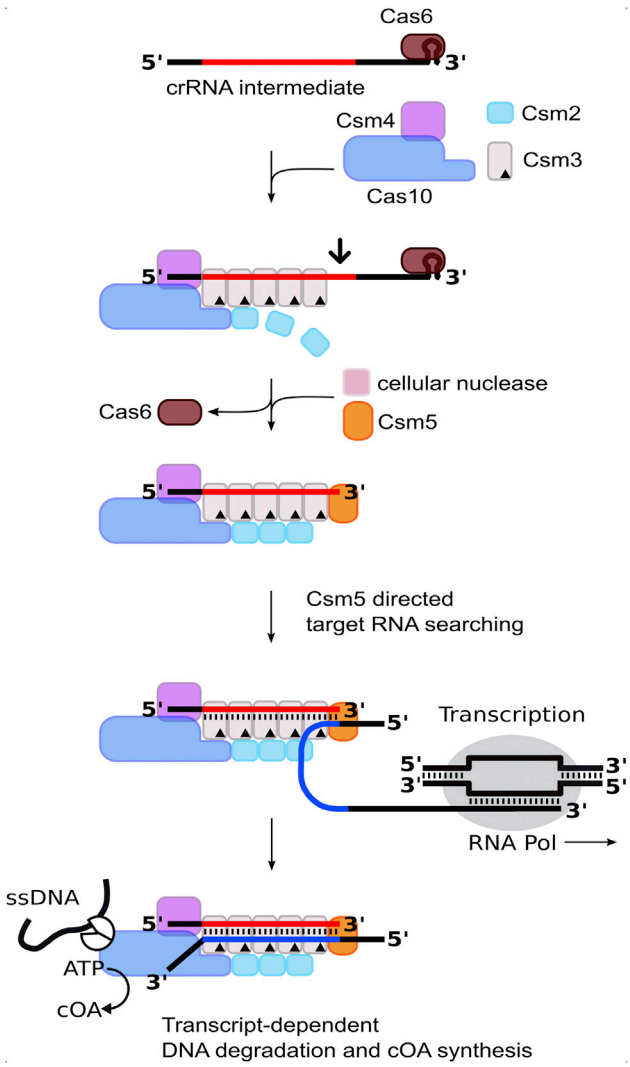

Figure 6. Cartoon Summary of the Csm Complex Assembly Model
Bold arrow indicates the 3′ end trimming of intermediate crRNA bound in the Csm effector complex by a cellular RNase. Triangles indicate RNase active sites of Csm3 subunits.

Csm5 Is Crucial for Target RNA Binding

It has been reported that in *S. epidermidis*, Csm5 facilitates crRNA maturation by recruiting cellular ribonuclease PNPase to the 3′ end of the crRNA (Walker et al., 2017). We showed here that in the absence of the Csm5 subunit, StCsm complexes exhibit decreased target and non-target RNA binding affinity, which can be restored by the addition of an isolated Csm5 protein (Figures 1D, 2, and S1D). This finding explains the previously reported ~10-fold reduced target RNA binding affinity of the StCsm-72 complex compared to the StCsm-40 complex (Tamulaitis et al., 2014). Given that ~90% of WT StCsm-72 complexes lack the Csm5 subunit that is required for target RNA binding, the observed binding of WT StCsm-72 is due to the remaining ~10% complex fraction containing the Csm5 subunit and exhibits the same binding affinity to target RNA as WT StCsm-40 (Figure 2). This finding demonstrates that Csm5 is crucial for target RNA binding, similarly to Cmr1 in the type III-B system from *S. solfataricus* (Li et al., 2017). Overall, these data implicate that in most CRISPR-Cas systems, additional domains or subunits are often required to initiate base-pairing between crRNA and the target sequence, as exemplified here by Csm5 for the type III and PAM (protospacer adjacent motif) or PFS (protospacer flanking site) interaction domains for type I, II, V, and VI systems (Leenay and Beisel, 2017).

Both single-molecule and biochemical studies revealed that a seed region is important for an RNA-guided target search by Argonautes and CRISPR effector complexes, such as Cas9 and Cascade (Globyte et al., 2018). UV cross-linking experiments of the StCsm-RNA complex revealed that the Csm5 subunit interacts with both target and nonspecific RNA (Figure S5). The Csm5 subunit alone also bound to a nonspecific RNA with high affinity (Figure S4A). Therefore, we propose that in type III systems, instead of seed recognition (Künne et al., 2014), Csm5 scans the emerging 5′ end of RNA transcripts for complementarity with crRNA, ensuring a rapid target site search in the transcript (Figure 6). Different cross-linking patterns of target and nonspecific RNAs indirectly supports this hypothesis; the nonspecific RNA cross-links only to the Csm5 subunit, while target RNA cross-links to both Csm5 and Cas10 subunits, implying different positions of RNAs in the specific and nonspecific StCsm complexes.

Cas6 Can Substitute for Csm5 in RNA Binding

ΔCsm5-1's affinity to target RNA is much higher than that of ΔCsm5-2 (Figure 2), suggesting an alternative target RNA binding pathway in the latter complex. The two ΔCsm5 complexes mainly differ by the presence of the Cas6 subunit in the ΔCsm5-1 complex (Figures 1B and S1B). Cas6 also cross-links to both target and nonspecific RNA (Figure S5), implying that Cas6 could partially substitute the Csm5 required for target RNA binding by the StCsm complex.

Cas6 binding to the target RNA impairs its interaction with the 3′ end of crRNA; therefore, non-target RNA binding triggers Cas6 release from crRNA, as illustrated for the ΔCsm5-1 mutant (Figure 2B). Indeed, the electrophoretic mobility of nonspecific Cas6 and ΔCsm5-1 RNA complexes is similar, implying that Cas6 is released from the complex after binding to the nonspecific RNA (Figures 2B and S3B). The addition of Csm5 to ΔCsm5-1 resulted in an increase in both specific and nonspecific RNA binding affinity. Again, the electrophoretic mobility of nonspecific Cas6 and ΔCsm5-1 RNA complexes is similar, implying that Cas6 is displaced from the StCsm complex by Csm5 addition (Figures 2C and S3C). Indeed, RNA binding by displaced Cas6 was confirmed by MS (Table S4). Therefore, we propose that the ΔCsm5-1 represents an intermediate stage in complex maturation in which Csm5 protein displaces Cas6 and invokes cellular ribonuclease to complete the processing of crRNA.

Cas10 Activity Depends on Target RNA Binding

In the StCsm effector complex, the HD and Palm domains of the Cas10 subunit are responsible for the DNase and cOA-synthase activity of the StCsm complex, respectively. Target RNA binding

by the StCsm complex induces both nonspecific ssDNA cleavage and cOA synthesis by the Cas10 subunit (Kazlauskiene et al., 2016, 2017). All subunit deletion variants containing the Cas10 subunit showed both Cas10-dependent activities depending on the target RNA binding affinity of the complexes (Figures 1F, 1G, S1F, and S1G). For example, ΔCsm5-1, which showed decreased target RNA binding, also demonstrated decreased DNase activity and cOA production that could be restored by increasing the target RNA concentration (Figure 1G).

Assembly of the Type III Effector Complex

Taken together, deletion analysis coupled with biochemical assays suggests the following speculative model for Csm complex assembly (Figure 6). Pre-crRNA is cleaved by Cas6 in the repeat region to produce ~72-nt-long crRNAs containing an 8-nt 5′-handle and a 28-nt 3′-handle. Our data indicate that Cas6 remains bound to the repeat sequence after the cleavage of R/1 RNA (Figures S3A). Cas10-Csm4 proteins form a subcomplex (Figure S2B) that presumably binds the 5′-handle of crRNA through the Csm4 subunit, similarly to Cmr3 in the Cmr complex (Osawa et al., 2015), to define the start position and initiate the assembly of other Csm proteins. Multiple cleavage positions of the target RNA at 1-nt intervals by the ΔCsm4 complex indirectly support this hypothesis (Figure 4). The crRNA accommodates at least five Csm3 subunits along its length. The inability to recover an StCsm complex in the absence of Csm3 (Figure 1B) is in good agreement with the StCsm structure model (Kazlauskiene et al., 2016) and Cmr crystal structure (Osawa et al., 2015), where Csm3 or Cmr4 subunits form a backbone of the complex. Similar results were obtained in the case of *S. epidermidis* ΔCsm3-SeCsm (Hatoum-Aslan et al., 2013, 2014). It is likely that the Cas10-Csm4 core recruits Csm3 subunits to crRNA to initiate their oligomerization. Next, Csm2 binding to the StCsm allows formation of the second intertwined helical protein filament. Indeed, Csm2 can be added to the pre-formed ΔCsm2 complex to restore the cleavage pattern (Figure 3B). The resultant immature Csm complex, as exemplified by our ΔCsm5-1 complex, is reminiscent of the type I-B, I-E, and I-F Cascade complexes, which contain Cas6 bound to the 3′ end of crRNA (Hochstrasser and Doudna, 2015). This supports a hypothesis that type I and III systems evolved from a common ancestral system (Mohanraju et al., 2016). Further binding of Csm5 displaces Cas6 and recruits cellular ribonuclease to process the 3′ end of crRNA (Walker et al., 2017), which results in the final maturation of the complex (Figure 6). It was suggested that the role of a ruler determining the length of matured crRNA is played by Csm3 (Hatoum-Aslan et al., 2013), but the detailed mechanism of this process remains to be elucidated.

Minimal Composition of StCsm

The matured StCsm complex that targets foreign NAs for destruction is composed of the Cas10:Csm2:Csm3:Csm4:Csm5 subunits and a 40-nt crRNA. Deletion analysis indicated that Csm2 and Csm5 subunits are dispensable for nuclease and cOA-synthase activities and that Cas10 can be omitted without impacting RNase activity. However, a minimal Csm complex composed of Csm3:Csm4:crRNA was unstable. Addition of the Cas10 subunit not only stabilized the minimal complex, resulting in notably increased complex yield, but also supported DNase and cOA-synthase activities. While the Cas10:Csm3:Csm4:crRNA complex exhibited decreased affinity toward RNA compared to WT, it cleaved both the target RNA and ssDNA and produced cOA (Figure 5).

The minimal StCsm complex is reminiscent of the type I-C minimal Cascade complex from *Desulfovibrio vulgaris*, which contains Cas7 (Csm3 analog), Cas5c (Csm4 analog), and Cas8c (large subunit, Cas10 analog) and a 64- to 68-nt crRNA (Hochstrasser et al., 2016). Further engineering efforts aimed to obtain fused Cas10-Csm4 variants or Csm4 variants with improved solubility may generate minimal type III effector complexes suitable for *in vivo* RNA manipulation both in prokaryotes and eukaryotes.

STAR★METHODS

Detailed methods are provided in the online version of this paper and include the following:

- KEY RESOURCES TABLE
- CONTACT FOR REAGENT AND RESOURCE SHARING
- EXPERIMENTAL MODEL AND SUBJECT DETAILS
- METHOD DETAILS
  - Construction of Single-Gene Deletion Mutants
  - Expression and Purification of Deletion Mutants
  - Expression and Purification of Minimal Complex
  - Expression of Cas10-Csm4 and Cas/Csm Proteins
  - Extraction and Length Analysis of crRNA
  - RNA and DNA Substrates
  - Electrophoretic Mobility Shift Assay
  - Mass Spectrometry
  - UV Cross-linking
  - RNA Cleavage Assay
  - DNA Cleavage Assay
  - Cyclic Oligoadenylate Synthesis Assay
- QUANTIFICATION AND STATISTICAL ANALYSIS

SUPPLEMENTAL INFORMATION

Supplemental Information can be found with this article online at https://doi.org/10.1016/j.celrep.2019.02.029.

ACKNOWLEDGMENTS

The authors thank Dalia Smalakyte, Georgij Kostiuk, and Arunas Silanskas for purification of proteins. We thank Ralf Seidel (Universität Leipzig) for critical reading of the manuscript and discussions. We also thank Audra Ruksenaite for MS analysis and discussions. This work was funded by a grant (APP-3/2016 to G.T.) from the Research Council of Lithuania. Publication of this article was funded by the Research Council of Lithuania.

AUTHOR CONTRIBUTIONS

I.M., M.K., and G. Tamulaitis designed research, and I.M., M.K., and S.V. performed research. I.M., M.K., G. Tamulaitiene, and G. Tamulaitis analyzed the data and wrote the paper. V.S. initiated the project, discussed the data, and revised the manuscript. All authors read and approved the final manuscript.

DECLARATION OF INTERESTS

M.K., G. Tamulaitis, and V.S. are inventors on patent applications related to the Csm complex. S.V. is an employee of Thermo Fisher Scientific Baltics, Lithuania. V.S. is a founder of CasZyme and a member of its scientific advisory board.

Received: July 13, 2018
Revised: December 29, 2018
Accepted: February 7, 2019
Published: March 5, 2019

REFERENCES

Benda, C., Ebert, J., Scheltema, R.A., Schiller, H.B., Baumgärtner, M., Bonneau, F., Mann, M., and Conti, E. (2014). Structural model of a CRISPR RNA-silencing complex reveals the RNA-target cleavage activity in Cmr4. Mol. Cell *56*, 43–54.

Carte, J., Wang, R., Li, H., Terns, R.M., and Terns, M.P. (2008). Cas6 is an endoribonuclease that generates guide RNAs for invader defense in prokaryotes. Genes Dev. *22*, 3489–3496.

Charpentier, E., Richter, H., van der Oost, J., and White, M.F. (2015). Biogenesis pathways of RNA guides in archaeal and bacterial CRISPR-Cas adaptive immunity. FEMS Microbiol. Rev. *39*, 428–441.

Elmore, J.R., Sheppard, N.F., Ramia, N., Deighan, T., Li, H., Terns, R.M., and Terns, M.P. (2016). Bipartite recognition of target RNAs activates DNA cleavage by the type III-B CRISPR-Cas system. Genes Dev. *30*, 447–459.

Estrella, M.A., Kuo, F.T., and Bailey, S. (2016). RNA-activated DNA cleavage by the Type III-B CRISPR-Cas effector complex. Genes Dev. *30*, 460–470.

Gasiunas, G., Barrangou, R., Horvath, P., and Siksnys, V. (2012). Cas9-crRNA ribonucleoprotein complex mediates specific DNA cleavage for adaptive immunity in bacteria. Proc. Natl. Acad. Sci. USA *109*, E2579–E2586.

Globyte, V., Kim, S.H., and Joo, C. (2018). Single-molecule view of small RNA-guided target search and recognition. Annu. Rev. Biophys. *47*, 569–593.

Han, W., Li, Y., Deng, L., Feng, M., Peng, W., Hallstrøm, S., Zhang, J., Peng, N., Liang, Y.X., White, M.F., and She, Q. (2017). A type III-B CRISPR-Cas effector complex mediating massive target DNA destruction. Nucleic Acids Res. *45*, 1983–1993.

Hatoum-Aslan, A., Maniv, I., and Marraffini, L.A. (2011). Mature clustered, regularly interspaced, short palindromic repeats RNA (crRNA) length is measured by a ruler mechanism anchored at the precursor processing site. Proc. Natl. Acad. Sci. USA *108*, 21218–21222.

Hatoum-Aslan, A., Samai, P., Maniv, I., Jiang, W., and Marraffini, L.A. (2013). A ruler protein in a complex for antiviral defense determines the length of small interfering CRISPR RNAs. J. Biol. Chem. *288*, 27888–27897.

Hatoum-Aslan, A., Maniv, I., Samai, P., and Marraffini, L.A. (2014). Genetic characterization of antiplasmid immunity through a type III-A CRISPR-Cas system. J. Bacteriol. *196*, 310–317.

Hochstrasser, M.L., and Doudna, J.A. (2015). Cutting it close: CRISPR-associated endoribonuclease structure and function. Trends Biochem. Sci. *40*, 58–66.

Hochstrasser, M.L., Taylor, D.W., Kornfeld, J.E., Nogales, E., and Doudna, J.A. (2016). DNA targeting by a minimal CRISPR RNA-guided Cascade. Mol. Cell *63*, 840–851.

Jackson, R.N., and Wiedenheft, B. (2015). A conserved structural chassis for mounting versatile CRISPR RNA-guided immune responses. Mol. Cell *58*, 722–728.

Jiang, W., Samai, P., and Marraffini, L.A. (2016). Degradation of phage transcripts by CRISPR-associated RNases enables type III CRISPR-Cas immunity. Cell *164*, 710–721.

Jinek, M., Chylinski, K., Fonfara, I., Hauer, M., Doudna, J.A., and Charpentier, E. (2012). A programmable dual-RNA-guided DNA endonuclease in adaptive bacterial immunity. Science *337*, 816–821.

Kazlauskiene, M., Tamulaitis, G., Kostiuk, G., Venclovas, Č., and Siksnys, V. (2016). Spatiotemporal control of type III-A CRISPR-Cas immunity: coupling DNA degradation with the target RNA recognition. Mol. Cell *62*, 295–306.

Kazlauskiene, M., Kostiuk, G., Venclovas, Č., Tamulaitis, G., and Siksnys, V. (2017). A cyclic oligonucleotide signaling pathway in type III CRISPR-Cas systems. Science *357*, 605–609.

Koonin, E.V., and Zhang, F. (2017). Coupling immunity and programmed cell suicide in prokaryotes: Life-or-death choices. BioEssays *39*, 1–9.

Koonin, E.V., Makarova, K.S., and Zhang, F. (2017). Diversity, classification and evolution of CRISPR-Cas systems. Curr. Opin. Microbiol. *37*, 67–78.

Künne, T., Swarts, D.C., and Brouns, S.J. (2014). Planting the seed: target recognition of short guide RNAs. Trends Microbiol. *22*, 74–83.

Leenay, R.T., and Beisel, C.L. (2017). Deciphering, communicating, and engineering the CRISPR PAM. J. Mol. Biol. *429*, 177–191.

Li, Y., Zhang, Y., Lin, J., Pan, S., Han, W., Peng, N., Liang, Y.X., and She, Q. (2017). Cmr1 enables efficient RNA and DNA interference of a III-B CRISPR-Cas system by binding to target RNA and crRNA. Nucleic Acids Res. *45*, 11305–11314.

Liu, T.Y., Iavarone, A.T., and Doudna, J.A. (2017). RNA and DNA targeting by a reconstituted Thermus thermophilus type III-A CRISPR-Cas system. PLoS ONE *12*, e0170552.

Mohanraju, P., Makarova, K.S., Zetsche, B., Zhang, F., Koonin, E.V., and van der Oost, J. (2016). Diverse evolutionary roots and mechanistic variations of the CRISPR-Cas systems. Science *353*, aad5147.

Niewoehner, O., Garcia-Doval, C., Rostøl, J.T., Berk, C., Schwede, F., Bigler, L., Hall, J., Marraffini, L.A., and Jinek, M. (2017). Type III CRISPR-Cas systems produce cyclic oligoadenylate second messengers. Nature *548*, 543–548.

Osawa, T., Inanaga, H., Sato, C., and Numata, T. (2015). Crystal structure of the CRISPR-Cas RNA silencing Cmr complex bound to a target analog. Mol. Cell *58*, 418–430.

Rouillon, C., Zhou, M., Zhang, J., Politis, A., Beilsten-Edmands, V., Cannone, G., Graham, S., Robinson, C.V., Spagnolo, L., and White, M.F. (2013). Structure of the CRISPR interference complex CSM reveals key similarities with Cascade. Mol. Cell *52*, 124–134.

Samai, P., Pyenson, N., Jiang, W., Goldberg, G.W., Hatoum-Aslan, A., and Marraffini, L.A. (2015). Co-transcriptional DNA and RNA cleavage during type III CRISPR-Cas immunity. Cell *161*, 1164–1174.

Sinkunas, T., Gasiunas, G., Waghmare, S.P., Dickman, M.J., Barrangou, R., Horvath, P., and Siksnys, V. (2013). In vitro reconstitution of Cascade-mediated CRISPR immunity in Streptococcus thermophilus. EMBO J. *32*, 385–394.

Spilman, M., Cocozaki, A., Hale, C., Shao, Y., Ramia, N., Terns, R., Terns, M., Li, H., and Stagg, S. (2013). Structure of an RNA silencing complex of the CRISPR-Cas immune system. Mol. Cell *52*, 146–152.

Staals, R.H.J., Agari, Y., Maki-Yonekura, S., Zhu, Y., Taylor, D.W., van Duijn, E., Barendregt, A., Vlot, M., Koehorst, J.J., Sakamoto, K., et al. (2013). Structure and activity of the RNA-targeting type III-B CRISPR-Cas complex of Thermus thermophilus. Mol. Cell *52*, 135–145.

Tamulaitis, G., Kazlauskiene, M., Manakova, E., Venclovas, Č., Nwokeoji, A.O., Dickman, M.J., Horvath, P., and Siksnys, V. (2014). Programmable RNA shredding by the type III-A CRISPR-Cas system of Streptococcus thermophilus. Mol. Cell *56*, 506–517.

Tamulaitis, G., Venclovas, Č., and Siksnys, V. (2017). Type III CRISPR-Cas immunity: major differences brushed aside. Trends Microbiol. *25*, 49–61.

Taylor, D.W., Zhu, Y., Staals, R.H., Kornfeld, J.E., Shinkai, A., van der Oost, J., Nogales, E., and Doudna, J.A. (2015). Structural biology. Structures of the CRISPR-Cmr complex reveal mode of RNA target positioning. Science *348*, 581–585.

Venclovas, Č. (2016). Structure of Csm2 elucidates the relationship between small subunits of CRISPR-Cas effector complexes. FEBS Lett. *590*, 1521–1529.

Walker, F.C., Chou-Zheng, L., Dunkle, J.A., and Hatoum-Aslan, A. (2017). Molecular determinants for CRISPR RNA maturation in the Cas10-Csm complex and roles for non-Cas nucleases. Nucleic Acids Res. *45*, 2112–2123.

Wei, W., Zhang, S., Fleming, J., Chen, Y., Li, Z., Fan, S., Liu, Y., Wang, W., Wang, T., Liu, Y., et al. (2019). Mycobacterium tuberculosis type III-A CRISPR/Cas system crRNA and its maturation have atypical features. FASEB J. *33*, 1496–1509.

Westra, E.R., van Erp, P.B., Künne, T., Wong, S.P., Staals, R.H., Seegers, C.L., Bollen, S., Jore, M.M., Semenova, E., Severinov, K., et al. (2012). CRISPR immunity relies on the consecutive binding and degradation of negatively supercoiled invader DNA by Cascade and Cas3. Mol. Cell *46*, 595–605.

Yoshioka, K. (2002). KyPlot—a user-oriented tool for statistical data analysis and visualization. Comput. Stat. *17*, 425–437.

STAR★METHODS

KEY RESOURCES TABLE

REAGENT or RESOURCE	SOURCE	IDENTIFIER
Bacterial and Virus Strains		
Escherichia coli BL21 (DE3)	Novagene	N/A
Chemicals, Peptides, and Recombinant Proteins		
SYBR Gold Nucleic Acid Gel Stain	Thermo Fisher Scientific	S11494
DNase I	Thermo Fisher Scientific	EN0521
RNase I	Thermo Fisher Scientific	EN0601
RNase A/T1	Thermo Fisher Scientific	EN0551
4-thio-UTP	Jena Bioscience	NU-1156S
[α^{32}P]-cordycepin-5′-triphospate	Perkin Elmer	NEG026250UC
[γ^{33}P]-adenosine-5′-triphospate	Perkin Elmer	N/A
T4 PNK	Thermo Fisher Scientific	EK0031
poly(A) polymerase	Thermo Fisher Scientific	AM2030
Ribolock RNase inhibitor	Thermo Fisher Scientific	EO0382
Critical Commercial Assays		
TranscriptAid T7 High Yield Transcription Kit	Thermo Fisher Scientific	K0441
Oligonucleotides		
crRNA^{40} 5′-ACGGAAACUUUCGUAACUGUUUAAUUCUGUUCACUUAUUC-3′	Metabion	N/A
Recombinant DNA		
pCas/Csm	Tamulaitis et al., 2014	N/A
pCRISPR_S3	Tamulaitis et al., 2014	N/A
pCsm2N-Tag	Tamulaitis et al., 2014	N/A
pCsm3N-Tag	Tamulaitis et al., 2014	N/A
pETDuet-1	Merck	71146
pCOLADuet-1	Merck	71406
pBAD24-Cas10C-His-StrepII-His	Kazlauskiene et al., 2016	N/A
M13mp18 single-stranded DNA	New England Biolabs	N4040S
Software and Algorithms		
Kyplot 2.0	Yoshioka, 2002	https://kyplot.software.informer.com/2.0/
Other		
Mass spectrometry analysis	Proteome Factory	https://www.proteome-factory.com/

CONTACT FOR REAGENT AND RESOURCE SHARING

Further information and requests for resources and reagents should be directed to and will be fulfilled by the Lead Contact, Virginijus Siksnys (siksnys@ibt.lt).

EXPERIMENTAL MODEL AND SUBJECT DETAILS

All StCsm complexes and proteins were expressed and grown in *Escherichia coli* BL21 (DE3) at 37°C in LB medium supplemented with appropriate antibiotics. The fresh LB medium was inoculated with an overnight culture (1/20 (v/v)), and bacteria were grown to the mid-log phase (OD600nm 0.5 to 0.7), then 1 mM IPTG and/or 0.2% (w/v) L-(+)-arabinose was added and cell suspension was further cultured for another 4 h.

METHOD DETAILS

Construction of Single-Gene Deletion Mutants

pCas/Csm plasmid carrying genes *cas6*, *cas10*, *csm2*, *csm3*, *csm4*, *csm5*, *csm6'* and *csm6* from *Streptococcus thermophilus* DGCC8004 CRISPR2 region (Tamulaitis et al., 2014) was used as a template to generate the following single-gene deletion mutant variants: pCas/Csm_ΔCas6, pCas/Csm_ΔCas10, pCas/Csm_ΔCsm4, and pCas/Csm_ΔCsm6'ΔCsm6 (see Table S1). To obtain the pCas/Csm_ΔCas6 variant, pCas/Csm plasmid was cleaved with Bsp1407I, the remaining sticky ends were blunted, phosphorylated (using "Fast DNA End Repair Kit" from Thermo Scientific), and ligated. This resulted in truncation of the cas6 gene from 243 to 67 codons. To obtain pCas/Csm_ΔCas10, a Bsp119I cleavage fragment was excised from the pCas/Csm plasmid. The re-ligated plasmid resulted in the *cas10* gene truncation from 758 to 185 codons. To obtain pCas/Csm_ΔCsm4, pCas/Csm was cleaved with SpeI and Eco31I, blunt-ended and re-ligated. This resulted in Csm4 ORF truncation from 299 to 41 codons. To obtain pCas/Csm_ΔCsm6'ΔCsm6, pCas/Csm was cleaved with PpiI and XmaJI, and resulting larger DNA fragment blunt-ended and subjected to ligation. This resulted in the Csm6' ORF truncation from 386 to 181 codons and elimination of Csm6 ORF.

To obtain pCas/Csm_ΔCsm5, a 2.7 kb DNA fragment containing *csm5*, *csm6'*, and *csm6* genes was subcloned from pCas/Csm plasmid into pUC18 vector, pre-cleaved with SphI and KpnI. The resulting pUC18_Csm5-Csm6'-Csm6 plasmid was then cleaved with SwaI and BsaAI. Thus derived larger DNA fragment was ligated to yield pUC18_ΔCsm5-Csm6'-Csm6 plasmid, containing a frameshift mutation at the start of the *csm5* gene. The SphI and PacI fragment, containing Δ*csm5*, *csm6'*, and *csm6*, was subcloned into the pCas/Csm plasmid to yield pCas/Csm_ΔCsm5.

pCas/Csm_Csm2 and pCas/Csm_ΔCsm3 were engineered using pUC18_Csm2-Csm3 plasmid carrying *csm2* and *csm3* genes. Briefly, first a 3.0 kb DNA fragment containing *csm2* and *csm3* genes was subcloned from pCas/Csm plasmid into the pUC18 vector pre-cleaved with SphI and KpnI to generate a plasmid pUC18_Csm2-Csm3. To obtain pCas/Csm_ΔCsm2, pUC18_Csm2-Csm3 was cleaved with BspMI and AflII, while to obtain pCas/Csm_ΔCsm3, ClaI and XhoI were used. The resulting large DNA fragments were then blunted, phosphorylated, and ligated to subclone them into pCas/Csm via NdeI and SpeI sites. This resulted in the Csm2 ORF truncation from 121 to 70 codons, and Csm3 ORF truncation from 220 to 57 codons, respectively. Full sequencing of cloned DNA fragments confirmed their identity to the expected sequences. In all cases, the deletions were executed in such a way that ribosome binding sites for other genes were not disrupted.

Expression and Purification of Deletion Mutants

Deletion mutant complexes were expressed and purified as described previously for the WT StCsm complex (Tamulaitis et al., 2014). Briefly, each mutant plasmid pCas/Csm with single-gene deletion was co-expressed in *Escherichia coli* BL21 (DE3) with pCRISPR_S3, containing five repeats interspaced by four identical spacers S3 (Tamulaitis et al., 2014), and pCsm2N-Tag or pCsm3N-Tag, coding Csm2 or Csm3 gene with StrepII-Tag fused to N-terminal (Tamulaitis et al., 2014) (see Table S1). Cells were harvested and disrupted, soluble deletion mutant StCsm complexes were captured by Strep-affinity chromatography via tagged Csm2 or Csm3 proteins, respectively, and subjected to size exclusion chromatography. The protein composition of the isolated deletion mutant complexes was analyzed by SDS–PAGE.

Expression and Purification of Minimal Complex

csm3 and *csm4* genes were cloned into pCDF-Duet-1 vector with a StrepII-Tag sequence at the N-terminal part of *csm3* to obtain pCsm3N-Tag_Csm4 plasmid. *cas6* gene was cloned into pCOLADuet-1 vector to obtain pCas6 plasmid. Minimal StCsm was obtained by co-expressing pCsm3N-Tag_Csm4 with pCas6 and pCRISPR_S3 in *Escherichia coli* BL21 (DE3). Expression of the complex was induced using 1 mM IPTG. Cells were harvested and disrupted, soluble complex was captured by Strep-affinity chromatography via tagged-Csm3 protein.

To increase the yield of the minimal complex, *cas10* was cloned into pETDuet-1 vector to obtain pCas10 plasmid. Further, we co-expressed pCsm3N-Tag_Csm4, pCas6, pCas10 and pCRISPR_S3 (Tamulaitis et al., 2014) in *Escherichia coli* BL21 (DE3). Expression of complex was induced using 1 mM IPTG. Cells were harvested and disrupted, soluble minimal StCsm complex (containing Cas6) was captured by Strep-chelating affinity via Strep-tagged Csm3. Complex was further subjected to size exclusion chromatography. The protein composition of the isolated minimal complex was analyzed by SDS–PAGE.

To eliminate Cas6 subunit from minimal StCsm we cloned *cas6* gene with N-terminal His-Tag sequence into pCOLADuet-1 to obtain pCas6N-Tag. pCas10 and pCas6N-Tag were co-expressed with pCsm3N-Tag_Csm4 and pCRISPR_S3. Expression of complex was induced with 1 mM IPTG. Min-StCsm (without Cas6) complex was purified by subsequent Strep-affinity, size exclusion and His-affinity chromatography.

Expression of Cas10-Csm4 and Cas/Csm Proteins

We cloned the *csm4* genes into pETDuet-1 vector and added a StrepII-Tag sequence to the N- or C-terminal part of *csm4* to obtain pCsm4N-Tag and pCsm4C-Tag plasmids, respectively. For expression of Csm4 constructed plasmids were expressed in *Escherichia coli* BL21 (DE3). Expression of Csm4 was induced using 1 mM IPTG at 37°C or 16°C.

We cloned the *csm4* genes into pCOLADuet-1 vector to obtain pCsm4 plasmid. For expression of Cas10-Csm4 subcomplex pCsm4 was co-expressed in *Escherichia coli* BL21 (DE3) together with pBAD24_Cas10C-His-StrepII-His plasmid (Kazlauskiene

et al., 2016). Expression of Cas10-Csm4 was induced using 0.2% arabinose and 1 mM IPTG. Subcomplex was purified using Strep-affinity chromatography.

We cloned the *csm5* and *cas6* genes into pETDuet-1 vector to obtain pCsm5N-Tag and pCas6C-Tag plasmids and added a StrepII-Tag sequence to the N-terminal part of *csm5* or C-terminal part of *cas6*. For expression of Csm2, Csm3, Csm5 and Cas6 proteins pCsm2N-Tag, pCsm3N-Tag (Tamulaitis et al., 2014), pCsm5N-Tag or pCas6C-Tag were expressed in *Escherichia coli* BL21 (DE3) (see Table S1 for summary of expression vectors). Expression of proteins was induced using 1 mM IPTG. Csm2, Csm3, Csm5 and Cas6 were purified using Strep-affinity chromatography.

Extraction and Length Analysis of crRNA

NAs copurified with StCsm complexes and StCsm proteins were isolated using phenol:chloroform: isoamylalcohol (25:24:1, v/v/v) extraction and precipitated with ethanol. Purified NAs were incubated with 0.8 U DNase I or 8 U RNase I (Thermo Scientific) for 30 min at 37°C. NAs were separated on a denaturing 15% PAGE and depicted with SYBR Gold (Thermo Scientific) staining.

RNA and DNA Substrates

Synthetic DNA oligonucleotides (Metabion) were used as PCR primers to generate transcription templates from pUC18_S3/1 (Tamulaitis et al., 2014). All RNA substrates were obtained by *in vitro* transcription using TranscriptAid T7 High Yield Transcription Kit (Thermo Scientific). A full description of all the DNA and RNA substrates is provided in Table S2. DNA and RNA substrates were either 5′-labeled with [γ^{33}P]-ATP (PerkinElmer) and T4 PNK (Thermo Scientific) or 3′-labeled with [α^{32}P]-cordycepin-5′-triphospate (PerkinElmer) and poly(A) polymerase (Thermo Scientific) followed by denaturing gel purification. M13mp18 single-stranded DNA plasmid was purchased from New England Biolabs.

Electrophoretic Mobility Shift Assay

Substrate binding assays were performed as described earlier (Tamulaitis et al., 2014). In brief, 0.5 nM of radiolabeled substrate was incubated with different amounts (0.01-300 nM) of each mutant complex in a binding buffer with EDTA. Reaction mixtures were analyzed by electrophoresis on native PAGE and depicted using a phosphorimager. After electrophoresis all gels were analyzed and the amounts of complexed and non-complexed RNA were determined using densitometric analysis. The K_D values for RNA binding by StCsm complex were calculated by fitting binding data to:

$$y = \left\{ s_0\text{-}x\text{-}K_d + \left[(s_0 + x + K_d)^2 \text{-} 4\ s_0 x \right]^{0.5} \right\} \Big/ 2 \quad (1)$$

where, y is the non-complexed RNA concentration (in terms of nM) evaluated from the gel at each StCsm complex concentration x (nM) put in the binding reaction, s_0 is the RNA concentration put in the binding mixture (we used 0.5 nM), and K_D is the dissociation constant calculated from the fit (nM).

Mass Spectrometry

Ten replicas of gel shifted bands "1" and "2" were cut from PAGE (Figure 2C) and sent for liquid chromatography mass spectrometry (LCMS) analysis, which was performed by Proteome Factory. Samples were eluted and proteins were cleaved with trypsin followed by separation and detection with LCMS.

UV Cross-linking

UV cross-linking reactions were performed similarly as described in (Spilman et al., 2013). Substrates for cross-linking were prepared using TranscriptAid T7 High Yield Transcription Kit (Thermo Scientific). RNA substrates used for UV cross-linking are provided in Table S2. 20 μL *in vitro* transcription reactions contained 200 ng of template DNA, 250 μM rUTP and 250 μM 4-thio-UTP (Jena Bioscience), 250 μM rATP and 4 μL of [α^{32}P]-ATP (800 Ci/mmol, 10 mCi/mL, Perkin Elmer); rGTP and rCTP were added to 500 μM final concentrations. Reactions were incubated for 8 hours at 37°C, followed by template DNA degradation by DNase I for 30 min at 37°C. Labeled RNA was isolated by ammonium acetate and ethanol precipitation. For UV cross-linking assays 400 nM thio-U-labeled RNA substrate and 500 nM StCsm were preincubated in 1X TAE buffer (40 mM Tris, 20 mM acetic acid (pH 8.4 at 25°C), 1 mM EDTA) at room temperature for 30 minutes. UV cross-linking was accomplished by irradiating the samples in fluorimeter by 356 nm UV light for 30 minutes. The complexes in cross-linked samples were denatured by addition of SDS to a final concentration of 1%, followed by incubation at 70°C for 10 minutes. The samples were incubated for 1 h at 37°C with RNase A/T1 Mix (2 μg/5 U respectively, Thermo Scientific). Proteins with cross-linked RNA were separated on 12% SDS-PAGE gel. Proteins were visualized by Coomassie G-250 (Thermo Scientific) staining and cross-linked RNA fragments were visualized by phosphorimaging and autoradiography.

RNA Cleavage Assay

Reactions were performed at 15°C and contained 4 nM of ^{33}P-5′-radiolabeled gel purified S3/1 or S3/6 RNA and 160 nM wt or mutant complex (or 320 nM in case of ΔCsm5 complexes) in Reaction buffer (33 mM Tris-acetate (pH 7.9 at 25°C), 66 mM K-acetate, 0.1 mg/ml BSA, 0.5 U/μl Ribolock (Thermo Scientific)). To evaluate RNA cleavage rate of Min-StCsm reactions were performed at

25°C and contained of 4 nM ^{33}P-5′-radiolabeled gel purified S3/6 RNA, 96 nM S3/6 RNA, 500 nM Min-StCsm or wt StCsm-40 complex in Reaction buffer. Reactions were initiated by addition of Mg-acetate to final concentration of 1 mM. Aliquots were removed at timed intervals and quenched with phenol. Aqueous phase was extracted using chloroform and mixed with 2x RNA loading buffer (Thermo Scientific) followed by incubation for 7 min at 85°C. The reaction products were separated on a denaturing 20% PAGE and depicted by autoradiography. Decline of RNA substrate over reaction time was evaluated by densitometric analysis, reaction rate constants k_{obs} for wt and deletion mutants were determined by fitting the data to single exponential. The decay of RNA cleavage by Min-StCsm was fitted to the two phase exponential decay:

$$y = Ae^{-k_1 x} + Be^{-k_2 x} + C \quad (2)$$

where, y – RNA substrate (in terms of %) evaluated from the gel at each reaction time x (s); A, B –fitted amplitudes (%) of different reacting species with rates k_1 and k_2, respectively; k_1, k_2 – reaction rates of different species calculated from the fit (s^{-1}); x – reaction time (s); C – amount of uncleaved substrate calculated from the fit (%).

DNA Cleavage Assay

Reactions were performed at 37°C and contained 2 nM of M13mp18 circular ssDNA (New England Biolabs) and 50 nM wt or mutant complex in the Reaction buffer with addition of 50 nM specific RNA substrate for DNA hydrolysis stimulation. In case of Min-StCsm, reactions contained 2 nM of circular ssDNA M13mp18, 500 nM Min-StCsm and 2000nM S3/20 or S3/6 RNA. Reactions were initiated by addition of $MnCl_2$ to final 10 mM concentration. The samples were collected at timed intervals and quenched by mixing 4 μL of reaction mixture with loading dye (95% v/v formamide, 0.01% bromophenol blue) followed by gel electrophoresis on a 1% agarose gel in 40 mM Tris, 20 mM acetic acid (pH 8.4 at 25°C), 1 mM EDTA buffer at 6 V/cm. DNA cleavage constants k_{obs} were determined by fitting single exponential to the substrate depletion data.

Cyclic Oligoadenylate Synthesis Assay

The synthesis reactions of cOAs by StCsm were initiated by adding 10 mM $CoCl_2$ into a mix of 200 nM StCsm complex, 200 nM or 2000 nM target RNA, 50 μM ATP and 10 nM [α^{32}P]-ATP in the Reaction buffer and carried out at 37°C for 1 h. In case of Min-StCsm, 500 nM Min-StCsm was mixed with 50 μM ATP and 10 nM [α^{32}P]-ATP without RNA or with 2000 nM S3/20 or S3/6 RNA in Reaction buffer. The reactions were stopped by adding 15 mM EDTA. Reaction products were separated by thin-layer chromatography (TLC) on PEI Cellulose F plates (Merck) in 0.325 M phosphate buffer (pH 3.5 at 23°C) and visualized using autoradiography.

QUANTIFICATION AND STATISTICAL ANALYSIS

Data analysis was performed using Kyplot 2.0 software (Yoshioka, 2002). Determined RNA binding and RNA and DNA cleavage rate constants are presented as the optimal value ± 1 standard deviation.